












Bismuth oxide-based nanocomposite for high-energy electron radiation shielding

Siyuan Chen¹ , Shruti Nambiar^{2,3,4} , Zhenhao Li¹ , Ernest Osei^{1,4,5,6} , Johnson Darko^{4,5,6} , Wanping Zheng⁷ , Zhendong Sun⁸ , Ping Liu⁹ , and John T. W. Yeow^{1,2,*} 

¹ Department of Systems Design Engineering, University of Waterloo, 200 University Ave. W., Waterloo, ON N2L 3G1, Canada

² Waterloo Institute of Nanotechnology, University of Waterloo, 200 University Ave. W., Waterloo, ON N2L 3G1, Canada

³ School of Pharmacy, University of Waterloo, 10A Victoria St. S., Kitchener, ON N2G 1C5, Canada

⁴ Department of Medical Physics, Grand River Regional Cancer Centre, Kitchener, ON N2G 1G3, Canada

⁵ Department of Physics and Astronomy, University of Waterloo, 200 University Ave. W., Waterloo, ON N2L 3G1, Canada

⁶ Department of Clinical Studies, Ontario Veterinary College, University of Guelph, 50 Stone Rd. E., Guelph, ON N1G 2W1, Canada

⁷ Space Science and Technology, Canadian Space Agency, 6767, Route de l'Aéroport, Saint-Hubert, QC J3Y 8Y9, Canada

⁸ Key Lab of Systems and Control, Academy of Mathematics and Systems Science, Beijing 100190, China

⁹ Dongguan University of Technology, Dongguan 523808, China

Received: 1 June 2018

Accepted: 23 October 2018

Published online:

30 October 2018

© Springer Science+Business Media, LLC, part of Springer Nature 2018

ABSTRACT

A novel polymer-based nanocomposite was fabricated to investigate its shielding properties against high-energy electron radiation for potential applications in space industry. Bismuth oxide (Bi_2O_3) nanoparticles and multi-walled carbon nanotubes (MWCNT) were added to poly (methyl methacrylate) (PMMA) to fabricate the nanocomposite. Radiation shielding efficiency of different samples, pure PMMA, PMMA/MWCNT, and PMMA/MWCNT/ Bi_2O_3 , was characterized and compared with aluminum (Al). The electron-beam attenuation characteristics show that PMMA/MWCNT/ Bi_2O_3 nanocomposite was 37% lighter in comparison with Al at the same radiation shielding effectiveness in electron energy range of 9–20 MeV. Furthermore, mechanical and thermal properties indicate that PMMA/MWCNT/ Bi_2O_3 can achieve significantly improved tensile strength, initial decomposition temperature, and glass transition temperature over pure PMMA. The stabled thermal properties, chemical structures, and morphology of all materials before and after electron irradiation lead to excellent radiation resistance of PMMA and nanocomposite. In conclusion, the proposed nanocomposite is a promising material for high-energy, electron-beam shielding applications.

Address correspondence to E-mail: jyeow@uwaterloo.ca

Introduction

The radiation environment in space consists of trapped radiation belts, cosmic rays, and solar energetic particles which is extremely hazardous to the health of astronauts and the electronics components in the spacecraft. Currently, most spaceflight missions are still around the Earth, such as the low Earth orbit (LEO), and the shielding provided by the Earth's magnetic field is capable of deflecting the major high-energy electron radiation that causes biomedical effects. However, future human space missions will extend to Moon base, habitations on Mars and even outer space. During such missions, electron radiation is one of the hazardous cosmic radiations, with energies up to tens of MeV, and capable of inducing carcinogenic effects in manned missions and/or serious damage to the spacecraft structural material and electronics components [1–5].

In order to maintain the functions of spacecraft electronics and the health of astronauts from the hazard radiations in manned missions, relatively high atomic number (Z) material, such as tantalum (Ta), through lower- Z material, aluminum (Al), have been applied [6–8]. Owing to high mechanical strength, low-cost and reliable fabrication process, Al is typically used for radiation shielding; however, its shielding effectiveness against high-energy electron radiation is limited by shielding effectiveness of the secondary bremsstrahlung photons that are produced by inelastic collisions of the electron radiation with the atomic nucleus of Al [9, 10]. Thus, to ensure the safety of personnel, more heavy material will be required for shielding, resulting in heavier payload and increasing mission cost and adversely affecting the mission duration due to more fuel consumption.

Alternatively, polymers which are usually composed of low- Z elements (such as hydrogen) with a weight advantage compared to metallic materials but capable of attenuating cosmic radiations without the massive production of secondary radiations are potential materials for space radiation shielding applications [11]. Pure polymers may not be effective shielding materials against high-energy electron radiation due to their low atomic number compounds when compared to the metal counterparts. However, addition of high- Z nanofillers in polymer matrix will gradually attenuate electron irradiation. Due to the low electron density of nanocomposite compared to metallic materials, high- Z nanoparticles

added nanocomposite will produce relatively low bremsstrahlung compared to metallic counterparts [11, 12]. Thus, the reinforcement of polymers with nanomaterials can result in improved electron attenuation characteristics of nanocomposites compared to Al [13–15].

The utilization of nanomaterials is one of the current trends in the aerospace industry. In recent studies, some groups have reported advantages of carbon-based nanomaterials (such as carbon nanotubes) as shielding materials against ionizing radiations [16–21]. It is reported that negligible deformations of MWCNT including radiation-induced formation of interstitial clusters and marginal shrinkage of inner carbon walls [18, 20]. By adding MWCNT into polymer matrix, compared to pure polymer, tensile strength of nanocomposite is able to be enhanced along with thermal stability due to formation of cross-linking sites and hindering effect under electron irradiation [22]. It indicates that MWCNT is able to stabilize thermal and mechanical properties of nanocomposite under electron-beam irradiation. In addition, studies investigating the potential of polymer composites for photon radiation shielding have shown that bismuth oxide (Bi_2O_3) has promising ability as nanomaterial reinforcement of polymers [23–25] and has also been demonstrated as safe alternative to lead (Pb) which is extremely toxic [23, 24]. Regarding shielding gamma radiation with energies lower than 2 MeV, Bi_2O_3 provides predominate function in polyester resin composites with uniform distribution [25]. However, as of yet, it has not been reported to use Bi_2O_3 as high-energy radiation absorber and/or shielding material for space applications.

Our group had previously reported that poly (methyl methacrylate) (PMMA) with three weight percentage (3 wt%) MWCNT nanocomposite (PMMA/MWCNT), compared to Al, was lighter, cost-effective, and a promising material to shield high-energy proton radiations in outer space [21]. In this study, we hypothesize that a hybrid nanocomposite including MWCNTs and high- Z nanoparticles dispersed in PMMA (PMMA/MWCNT/ Bi_2O_3) can effectively attenuate electron beams with energies of 9–20 MeV similar to those reported for outer space [5, 26]. The PMMA/MWCNT/ Bi_2O_3 nanocomposite has been characterized using thermogravimetric analysis (TGA), differential scanning calorimetry (DSC), Fourier-transform infrared (FTIR)

spectroscopy and scanning electron microscope (SEM) and the attenuation properties under electron beams have been investigated. Advantages of PMMA/MWCNT/Bi₂O₃ nanocomposite have been discussed and compared with Al, pure PMMA, and our previously developed PMMA/MWCNT nanocomposite.

Methods

PMMA with MWCNT and Bi₂O₃ nanocomposites (PMMA/MWCNT/Bi₂O₃) were fabricated, and the composition is 3 wt% of MWCNT, 30 wt% of Bi₂O₃, and 67 wt% of PMMA. Increasing weight percentage of Bi₂O₃ in composites has proven to be capable of achieving improved radiation shielding performance [27–29]. However, radiation shielding effectiveness or weight advantage threshold may be reached when increasing weight percentage of Bi₂O₃ above 30%. To adopt the best radiation shielding property and maintain the uniform dispersion quality in nanocomposite, 30 wt% of Bi₂O₃ was applied in our nanocomposite. In this study, its material properties such as thermal decomposition, glass transition temperature, chemical structure, and dispersion were characterized. Pure PMMA, PMMA/MWCNT, and aluminum were used as reference materials.

Fabrication

Research grade PMMA powders (Sigma-Aldrich, #182230), MWCNT (Nanostructured & Amorphous Materials, –COOH, 95+%, OD 10–20 nm), and Bi₂O₃ nanoparticles (Sigma-Aldrich, #202827) were used for the fabrication and tests. Melt mixer (Haake Rheocord 90) and hot press instrument were used for fabrication of pure PMMA, PMMA/MWCNT, and PMMA/MWCNT/Bi₂O₃ nanocomposite. PMMA powder (micron-sized particles) were heated and melted at 200 °C in the mixer followed by addition of 3 wt% of MWCNT. Subsequently, 30 wt% of Bi₂O₃ nanoparticles was added to the molten mixture. PMMA samples were then loaded into the hot press at 180 °C and pressure of 1.6 MPa; the press is used for molding thermoplastics into solid squares 30 × 30 cm². As shown in Fig. 1, pure PMMA, PMMA/MWCNT, and PMMA/MWCNT/Bi₂O₃ were cut into 3.5 × 3.5 cm plates by laser cutter (VLS 2.30, Universal laser systems).

Characterization studies

Pure PMMA, PMMA/MWCNT, and PMMA/MWCNT/Bi₂O₃ samples were characterized with tensile strength tester, TGA, DSC, FTIR, and SEM. All those samples were measured before and after electron-beam irradiation in order to determine radiation effects on the thermal properties, chemical structure, and/or any visible morphological changes in the materials.

In terms of mechanical property of materials, the tensile strengths of both the irradiated and non-irradiated samples were measured with an Instron 5548 Micro Tester following the ASTM standard of D638-10. Samples were prepared with the required shape and dimensions with the laser engraving system.

TGA apparatus was used to identify components and thermal degradation process of materials with programmed temperature. The test temperature was set as increasing from room temperature to 800 °C with ramp of 20 °C/min under nitrogen environment in TA instrument Q500. Weight of materials was monitored in real time to compare the thermal degradation as a function of increase in temperature.

DSC is an important method to measure the glass transition temperatures (*T_g*) of polymer materials. Samples were tested in a sealed chamber in TA Q2000 under 25–180 °C at ramp rate of 10 °C/min followed by decreasing rate of 20 °C/min from 180 °C to room temperature. Heat transition through samples over raising temperature can be plotted to analyze modified *T_g* in composite compared to pure polymer.

FTIR spectroscopy can be used to represent a molecular ‘fingerprint’ of the sample and observe some chemical structure change in composites. Tested samples were grinded into micro-sized powders used to form pellets with potassium bromide (KBr) under pressure. All materials were prepared at the same concentration and dried in vacuum oven overnight before testing with IR radiation.

Moreover, SEM images were acquired using Zeiss Ultra plus SEM. Samples were coated with a thin layer of gold (20 nm) to improve image quality. Surface microstructure of nanocomposites was evaluated at a magnitude of 12kX.

Electron-beam attenuation test

Figure 2 shows the setup of the electron-beam irradiation of the sample materials. All measurements

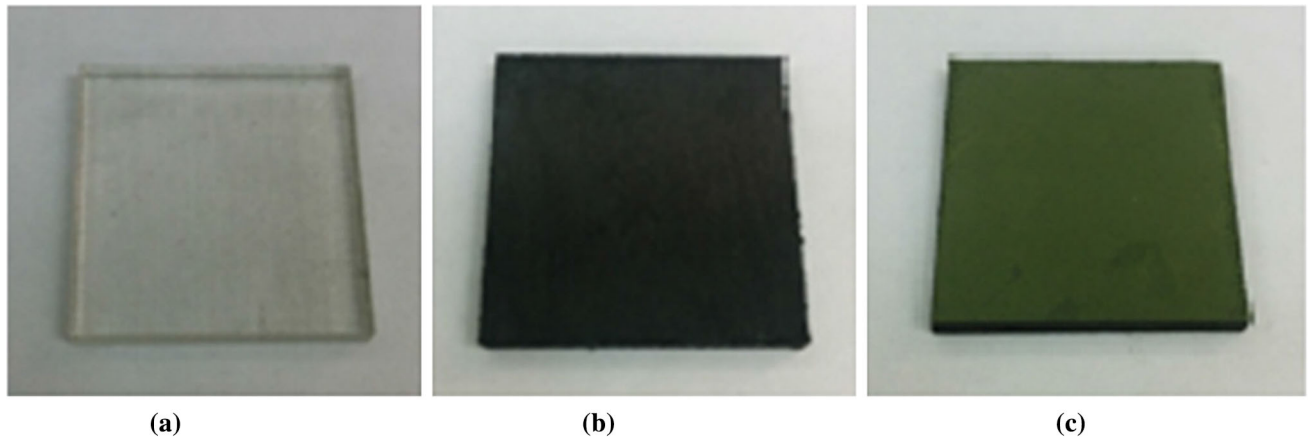


Figure 1 a Pure PMMA, b PMMA/3 wt% MWCNT, c PMMA/3 wt% MWCNT/30 wt% Bi₂O₃.

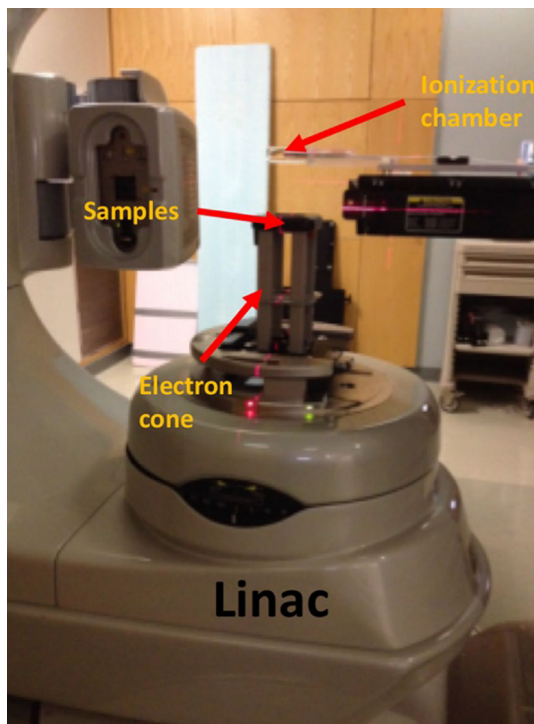


Figure 2 Electron irradiation test setup.

were done using a Clinac[®] 21EX System machine at the Grand River Regional Cancer Centre (Kitchener, ON, Canada). The dose delivered to each sample was 100 monitor unit (MU) (100 cGy) at a dose rate of 1000 MU/min for this work. A 6 × 6 cm² electron cone applicator with 3 cm diameter lead cutout insert was used for the electron-beam irradiation. Pure PMMA (reference material), PMMA/MWCNT (nanocomposite), PMMA/MWCNT/Bi₂O₃ (nanocomposite), and Al (reference material) were used to study the electron-beam attenuation

characteristics for electron-beam energies of 9, 12, 16, and 20 MeV. The samples were placed at the end of the electron cone with the aid of a holder. The distance between the electron source/target and the irradiated samples holder was at 95 cm from the source as shown in Fig. 2. Various samples with different thicknesses were placed on the sample holder to investigate the attenuation properties. An ionization chamber (Farmer chamber), positioned at a distance of 110 cm from the electron target, was used to measure the transmitted electrons beam through the sample. An ion chamber reading without the sample in place was first taken as a baseline reading. For purposes of this study, the ion chamber reading can be denoted as C_t when a sample is placed between the source and the chamber reading, C_0 when there is no sample in place. Then the relative electron attenuation (%) of the samples can be calculated as: $\eta = ((C_0 - C_t)/C_0) \times 100\%$. The attenuation results are plotted as a function of areal density (A) derived from the product of mass density (ρ) and thickness (t) of the material ($A = \rho \times t$). In this study, areal density is indicative of the weight required to stop programmed electron-beam energy for each material. Thus, it is used to compare weight advantages between nanocomposites and reference materials such as Al. Transmission characteristics for five different areal densities (0.58 g/cm², 1.00 g/cm², 1.44 g/cm², 3.60 g/cm², and 6.43 g/cm²) of each sample irradiated at four different electron-beam energies (9, 12, 16, and 20 MeV) were measured. At the same electron attenuation percentage (η), weight advantages of samples over Al can be calculated as: $D = ((A_{\text{aluminum}} - A_{\text{sample}})/A_{\text{aluminum}}) \times 100\%$.

Results and discussion

Material characterization

The tensile strength results are given in Fig. 3. Efficiently stress transfer at the particle/polymer interface is the most important factor to improve mechanical strength of nanocomposite [30]. The addition of homogeneously dispersed nanomaterials has shown improved mechanical property in PMMA matrix. Compared to pure PMMA, PMMA/MWCNT and PMMA/MWCNT/Bi₂O₃ are showing about 35% and 37.7% increase in tensile strength, respectively.

The TGA results are shown in Fig. 4. The first 2% weight loss of all materials can be considered as removal of contaminants during the degassing process followed by a plateau and subsequently starts to drop around 210 °C with increasing temperature. Based on the TGA data, 98% of total weight of PMMA/MWCNT is left at 237 °C, the starting temperature for material decomposition (initial decomposition temperature) which is 27 °C higher than that of pure PMMA (210 °C). Moreover, the nanocomposite with Bi₂O₃ nanoparticles showed significant thermal stability improvement such that the initial decomposition temperature (278 °C) is about 68 °C (about 32.4%) higher than that of the pure PMMA. This is caused by the high thermal stability of the homogeneously distributed Bi₂O₃ nanoparticles, and also the MWCNT in polymer matrix restrained the degradation of PMMA chains during pyrolysis [31–35].

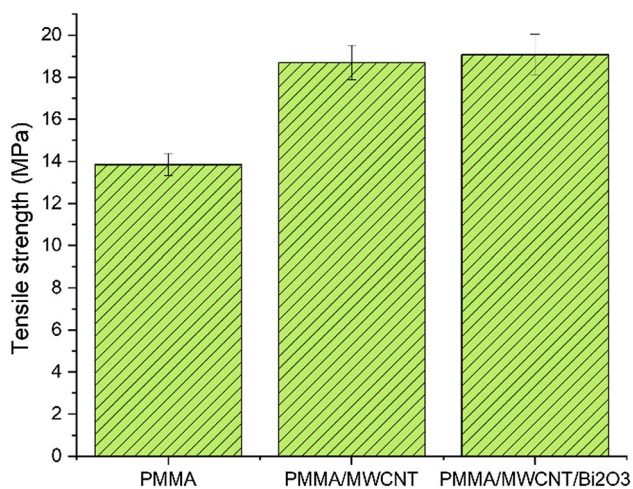


Figure 3 Tensile strength data of the fabricated samples.

Compared to the non-irradiated samples, the initial decomposition temperature of electron-beam irradiated samples (PMMA: 211 °C, PMMA/MWCNT: 235 °C, PMMA/MWCNT/Bi₂O₃: 276 °C) differed by only less than 1%, which suggests that irradiated samples (PMMA: 210 °C, PMMA/MWCNT: 237 °C, PMMA/MWCNT/Bi₂O₃: 278 °C) maintain their thermal properties.

On the other hand, about 33 wt% and 3 wt% of residual material of PMMA/MWCNT/Bi₂O₃ and PMMA/MWCNT, respectively, remained when temperature increased above 425 °C. For pure PMMA, almost no residual was found at temperatures > 425 °C; the polymer was totally decomposed. Since the nanomaterials (Bi₂O₃ and MWCNT) are highly heat resistant, the residual weight percentages (33 wt% and 3 wt%) precisely indicate the original weight percentages of MWCNT and Bi₂O₃ in PMMA/MWCNT/Bi₂O₃ and MWCNTs in PMMA/MWCNT.

DSC data of both electron-beam irradiated and non-irradiated materials are shown in Fig. 5. Both nanomaterials, MWCNT and Bi₂O₃, largely improve the *T_g* of pure PMMA. PMMA/MWCNT/Bi₂O₃ nanocomposite has considerably higher *T_g*: 13.3% and 3.5% than pure PMMA and PMMA/MWCNT, respectively. It is evident that the nanofillers can potentially enhance the working temperature range of the nanocomposites making them ideal candidates for space applications. For example, the radiation shielding components, used in space missions in the low Earth orbit, require a wide range of working temperatures (up to 100 °C) in order to avoid potential risks of thermal degradation due to the harsh environment [36]. Post radiation, *T_g* of PMMA and nanocomposites dropped less than 1 °C. This minor change may be caused by minimal/low interaction of the high-energy electrons with the samples such that the thermal properties remained unaltered [37].

FTIR was used to investigate interactions between nanoparticles and PMMA polymer chain in nanocomposites before and after electron irradiation. As shown in Fig. 6, both nanocomposites (PMMA/MWCNT and PMMA/MWCNT/Bi₂O₃) have shown intensity changes in the range of 600–1100 cm⁻¹ results in the formation the linkages between carbon and PMMA. Around 987 and 750 cm⁻¹, increased density with respect to both nanocomposites has shown additional C atoms in PMMA polymer chain

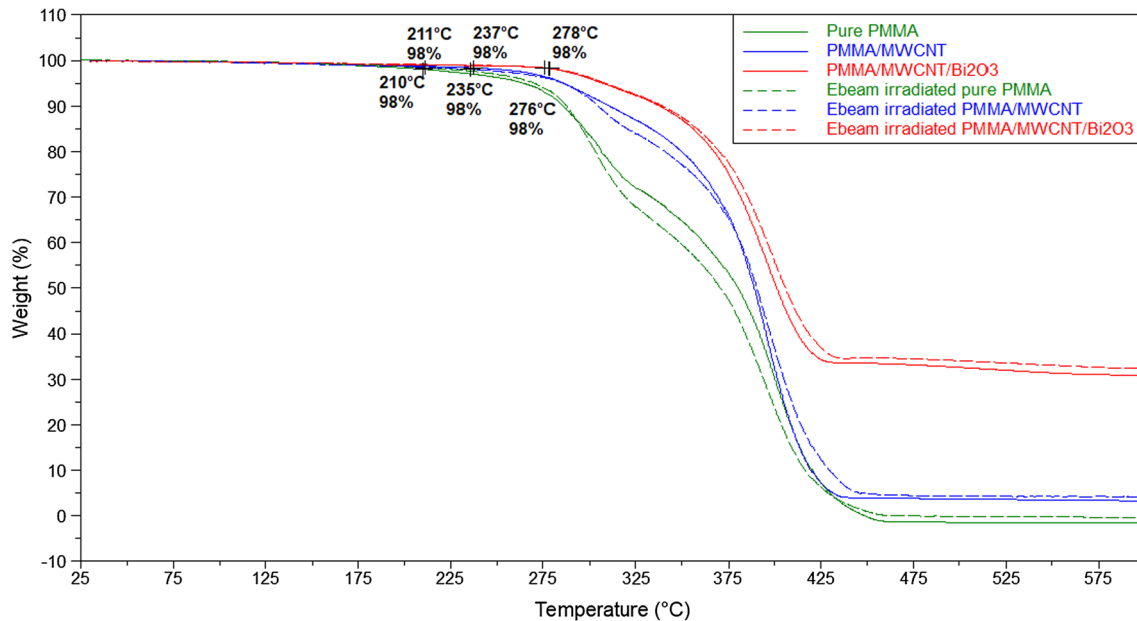


Figure 4 TGA data of samples before and after irradiation of electron beam.

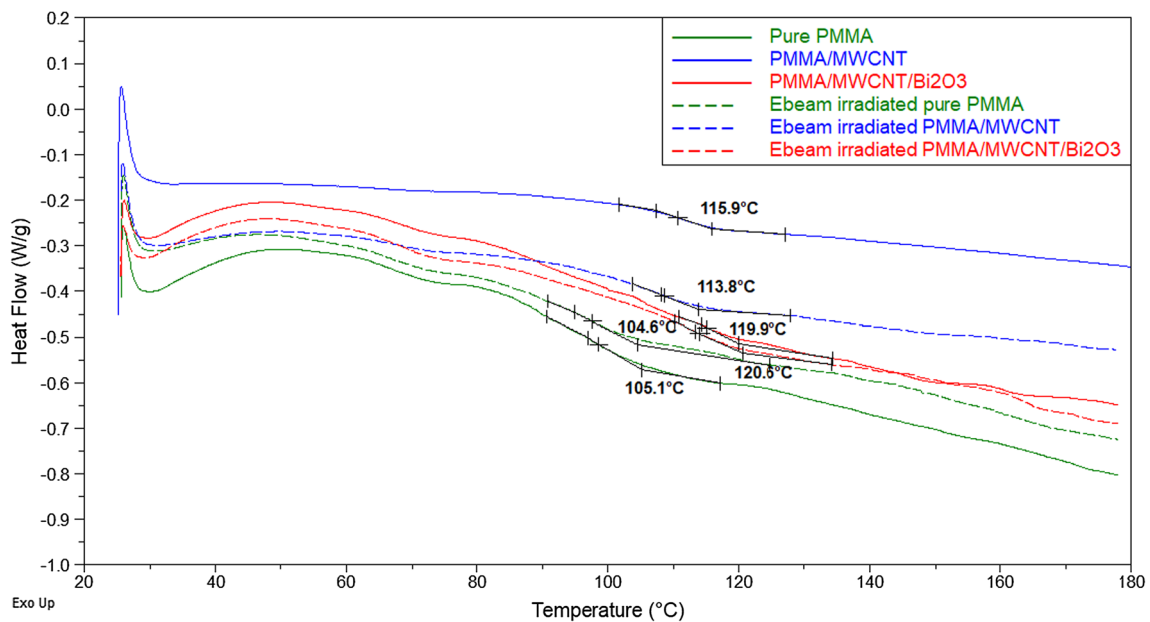


Figure 5 DSC data of samples before and after electron radiation.

[38, 39]. However, addition of Bi_2O_3 has shown less intensity changes compared to PMMA/MWCNT due to less PMMA chains in the nanocomposite. Besides that, all materials have not indicated significant chemical structure changes after high-energy electron radiation tests.

SEM images of PMMA/MWCNT/ Bi_2O_3 before and after electron-beam irradiation are shown in Fig. 7. The uniformly distributed spherical particles

represent Bi_2O_3 nanoparticles surrounded by bright web-like structure of the MWCNTs. No sign of aggregation of MWCNT is observed in all images, demonstrating uniform dispersion of nanomaterials in the PMMA matrix. The SEM images of PMMA/MWCNT/ Bi_2O_3 cross sections before and after electron-beam irradiation show no obvious deformations including radiation-induced polymer matrix

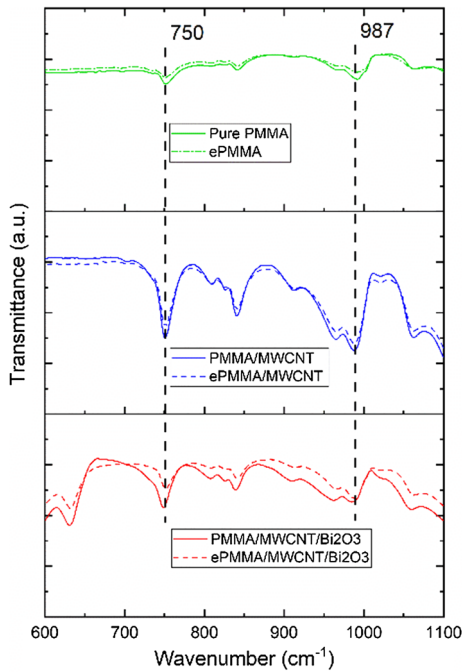


Figure 6 FTIR spectrum of the samples before (solid lines) and after (dash lines) electron irradiation (e represents electron irradiated in the graph).

degradation that can lead to exposure and aggregation of MWCNT [40, 41].

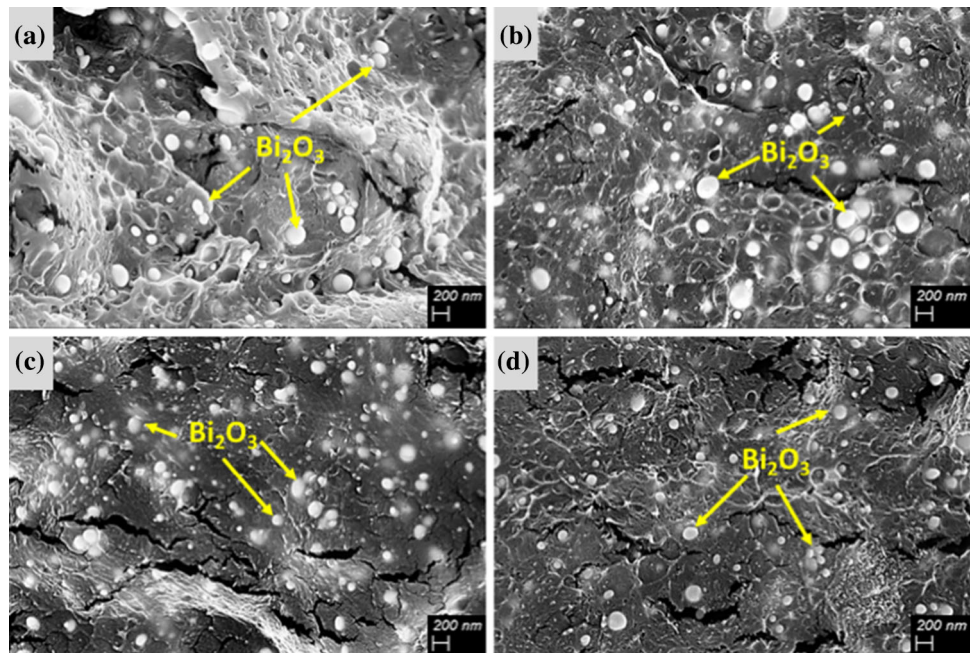
Several studies have been reported on radiation-induced chain scission and/or cross-linking effects in polymers, such as PMMA [42–44]. However, compared to 20 Gy in this study, those drastically

changed mechanical and thermal properties of polymers can be induced by higher radiation dose (several kGy). Thus, the chain scission and cross-linking effects were less likely to have occurred in our irradiated samples.

Electron-beam attenuation test

Besides the radiation resistance property, electron attenuation characteristics of developed materials are discussed. The percentage attenuation characteristics for each of the four energies (9, 12, 16, and 20 MeV) are shown in Fig. 8. As the electron-beam energy increases from 9 to 20 MeV, more materials for each sample were required to attenuate the electron beam. As shown in Fig. 8, the attenuation for all materials increases with increase in areal density and then saturate at higher areal densities. The percentage attenuation characteristic of PMMA/MWCNT nanocomposite is similar to the control sample (PMMA), and the overall trend of materials was found to be similar for all energies. However, the PMMA/MWCNT/Bi₂O₃ nanocomposite shows better shielding properties than the other materials for any given areal density. To achieve equivalent electron shielding performance, the nanocomposite shielded better and required less amount of material in comparison to Al. For example, at 94% attenuation under 9 MeV electron beam, the PMMA/MWCNT/Bi₂O₃ nanocomposite was about 33.33% lighter than

Figure 7 SEM images of PMMA/MWCNT/Bi₂O₃ nanocomposites before (a, c) and after (b, d) electron-beam irradiation.



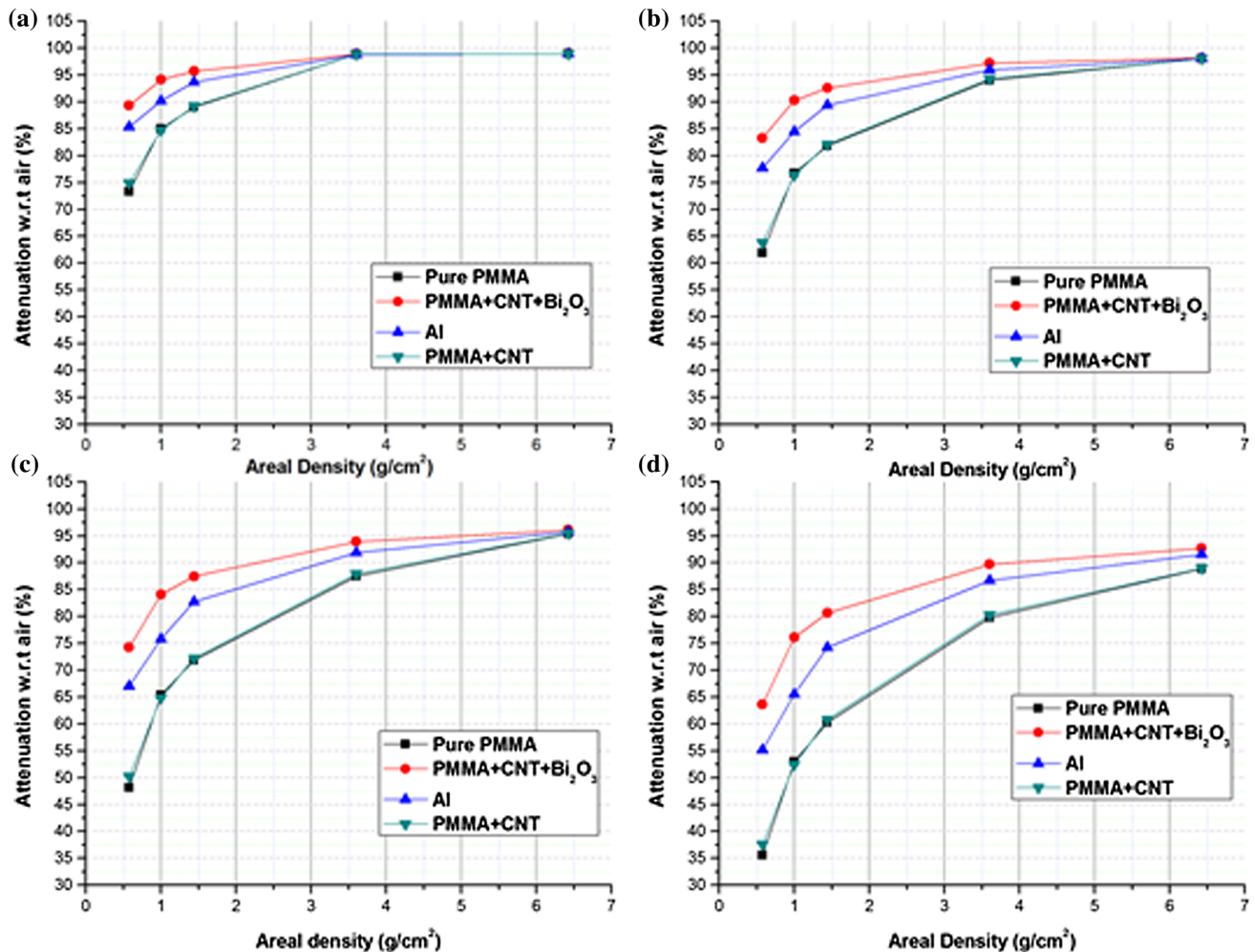


Figure 8 Percentage attenuation of all materials at a 9 MeV, b 12 MeV, c 16 MeV, d 20 MeV.

Al. Of all the materials, the PMMA/MWCNT/Bi₂O₃ nanocomposite was found to be the lightest for given exposure.

Besides that, under electron radiation with energy of 9 MeV, maximum electron attenuation of 98% for all shielding materials is infinitely approached at areal densities above ~ 3.3 g/cm² (shown in Fig. 8). The areal density of 3.3 g/cm² is denoted as saturated point of areal density for 9 MeV electron radiation. As a result, increasing thickness of shielding materials over saturated point will no longer improve electron attenuation effectiveness. This phenomenon is observed in other electron energies as well (12, 16, and 20 MeV). One reason is that continuous slowing down approximation (CSDA) ranges of Al and PMMA (5.33 and 4.67 g/cm² at 9 MeV electron beam, respectively) suggest, beyond areal density of 3.3 g/cm², few existing primary electrons still contribute

the 2% unshielded radiations [45]. Secondly, generated by the interactions between primary electrons and shielding materials as well as other components in the experiment setup, secondary radiations such as bremsstrahlung photons and Auger electrons were counted [15]. At each electron shielding saturated point, a noticeable phenomenon was found that the maximum attenuation percentages at saturated points decrease accordingly when primary electron-beam energy increases from 9 to 20 MeV. In other words, greater quantity of transmitted primary electrons and secondary radiations can be detected when more shielding materials are used at higher electron energies.

Besides that, as illustrated in Fig. 9, areal densities of saturated points as a function of all four electron energies were plotted to investigate saturated points for the all electron energies. The linear relationship

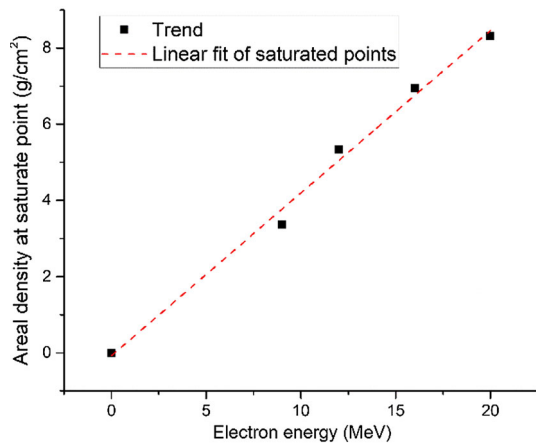


Figure 9 Linear fit of saturated points for all energies.

between them is presented, but electron energy of 9 MeV is showing slightly drifting from the other points. Potentially, this plot is able to predict saturated areal densities for electron radiation shielding at other electron energies than the four measured in this study.

Moreover, according to the plots in Fig. 8, the maximum weight advantages of PMMA/MWCNT/Bi₂O₃ at various electron irradiation energies are found and listed in Table 1. The attenuation characteristics of all the materials as a function of different areal densities and energies show that the PMMA/MWCNT/Bi₂O₃ nanocomposite would be much lighter material than Al for electron radiation shielding. For instance, at electron energy of 9 MeV, the nanocomposite is found to have maximum 37.49% weight advantage in comparison with Al at electron-beam attenuation of 90%, which is found to be the best shielding characteristics of the nanocomposite (PMMA/MWCNT/Bi₂O₃) for all measured energies. However, around 37% weight advantage compared to Al is observed regardless of electron energy. Moreover, it is adverted that electron attenuation percentages at the greatest weight advantages

of nanocomposite decrease accordingly when the primary electron-beam energy goes up, which has a similar trend as the maximum attenuation percentages at the saturated points.

For each of the areal densities, the percentage attenuation behavior was plotted as a function of increasing energy (Fig. 10). For all areal densities, the PMMA/MWCNT/Bi₂O₃ nanocomposite showed advantages over Al. However, the PMMA/MWCNT/Bi₂O₃ nanocomposite shows higher attenuation of electron beam compared to Al at lower areal densities. At areal densities < 3.6 g/cm² (Fig. 10a, b, c), compared to areal density of 3.6 and 6.43 g/cm², PMMA/MWCNT/Bi₂O₃ showed higher attenuation advantage (≥ 5%) over Al at all the energies used in this study. Regarding areal density of 6.43 g/cm², PMMA/MWCNT/Bi₂O₃ nanocomposite shows attenuation advantages at higher electron-beam energies (16 and 20 MeV). Nevertheless, at lower energies (9 and 12 MeV), all materials reach the same attenuation characteristics. As discussed above, this is because that areal density of 6.43 g/cm² has reached and exceeded electron shielding saturated points for radiation energies of 9 and 12 MeV, where all materials show minor or the same electron attenuation percentage.

Conclusion

In space applications, Al constructed units used for protecting radiation-sensitive components from ionizing space radiations, such as electrons, will open the way for innovative material with light-weight advantage. The present research has demonstrated that Bi₂O₃ added hybrid nanocomposite possesses greater than 70% electron attenuation at electron-beam energies ranging from 9 to 20 MeV when maximum weight advantage (around 37%) compared to Al is achieved. The weight advantage of

Table 1 Weight advantage with respect to Al for all energies

Electron energy (MeV)	Maximum percentage weight reduction (%)	Areal density of nanocomposite at the max weight reduction (g/cm ²)	Attenuation at the greatest weight advantage (%)
9	37.49	0.61776	90
12	36.34	0.76769	87
16	36.16	0.58903	75
20	36.30	0.76862	70

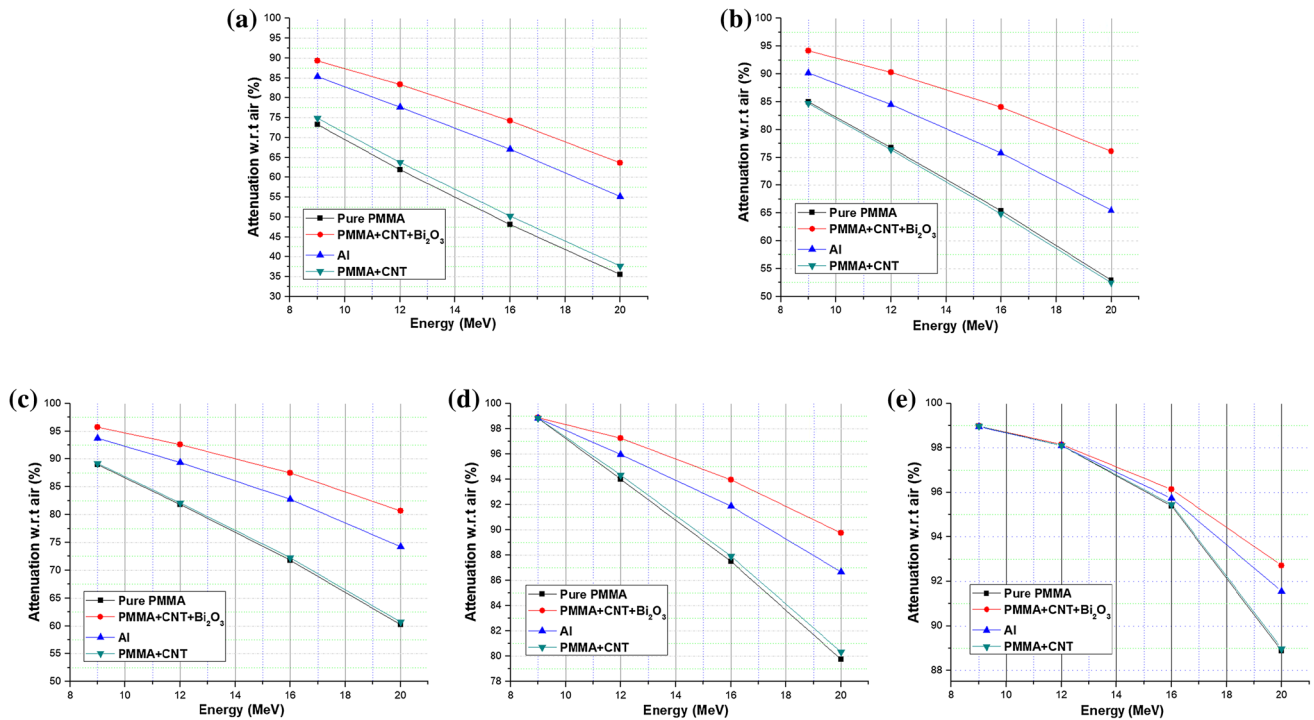


Figure 10 Percentage attenuation as a function of energy at areal density of **a** 0.58 g/cm², **b** 1.00 g/cm², **c** 1.44 g/cm², **d** 3.60 g/cm², and **e** 6.43 g/cm².

nanocomposite is showing slightly higher value (37.49%) at lower electron-beam energies (9 MeV); however, it is found that nanocomposite has no weight advantage if areal density of shielding materials reaches saturated point. For instance, all materials with areal density greater than 3.3 g/cm² can achieve the same 98% electron attenuation under 9 MeV electron-beam radiation. Besides that, saturated points of materials are linear to all electron-beam energies. Based on the characterization results, tensile strength and thermal stability (TGA and DSC) of PMMA are considerably improved by addition of homogeneously dispersed MWCNT and Bi₂O₃ nanoparticles. Moreover, deformations of nanocomposites after electron irradiation are barely found from thermal property tests, FTIR, or SEM images. This work has indicated that PMMA/MWCNT/Bi₂O₃ nanocomposite is promising in aerospace applications. Incorporating with our previous study, a multilayer design with the two nanocomposites (PMMA/MWCNT and PMMA/MWCNT/Bi₂O₃) can potentially be developed to shield both high-energy proton and electron radiations in future research.

Acknowledgements

This research was supported by Natural Sciences and Engineering Research Council of Canada (NSERC) and Canadian Research Chairs (CRC).

References

- [1] Grossman E, Gouzman I (2003) Space environment effects on polymers in low earth orbit. *Nucl Instrum Methods Phys Res Sect B Beam Interact Mater Atoms* 208:48–57
- [2] Lin R (2000) Energetic electrons accelerated in solar particle events. In: *AIP conference proceedings*, vol 528, no. 1, pp 32–38. AIP
- [3] Webber W, Villa T (2017) The galactic cosmic ray electron spectrum from 3 to 70 MeV measured by Voyager 1 beyond the heliopause, what this tells us about the propagation of electrons and nuclei in and out of the galaxy at low energies. *arXiv preprint arXiv:1703.10688*
- [4] Charlesby A (2013) *Atomic radiation and polymers: international series of monographs on radiation effects in materials*. Elsevier, Amsterdam
- [5] Bolton S et al (2002) Ultra-relativistic electrons in Jupiter's radiation belts. *Nature* 415(6875):987

- [6] Smith DM et al (2002) The RHESSI spectrometer. *Sol Phys* 210(1–2):33–60
- [7] Cucinotta FA (2015) Review of NASA approach to space radiation risk assessments for Mars exploration. *Health Phys* 108(2):131–142
- [8] Pia MG et al (2009) PIXE simulation with Geant4. *IEEE Trans Nucl Sci* 56(6):3614–3649
- [9] International Commission on Radiation Units and Measurements (1984) Radiation dosimetry: electron beams with energies between 1 and 50 MeV; 2nd reprint. International Commission on Radiation Units and Measurements, Bethesda
- [10] Dapor M (2003) Electron-beam interactions with solids: application of the Monte Carlo method to electron scattering problems. Springer, Berlin
- [11] Adams J Jr et al (2005) Revolutionary concepts of radiation shielding for human exploration of space
- [12] Chandrika BM, Manjunatha HC, Sridhar KN, Hanumantharayappa C (2018) Bremsstrahlung shielding parameters in polymer concretes. *Radiat Effects Defects Solids*. 26:1–3
- [13] Thibeault SA, Kang JH, Sauti G, Park C, Fay CC, King GC (2015) Nanomaterials for radiation shielding. *MRS Bull* 40(10):836–841
- [14] Li Z, Nambiar S, Zheng W, Yeow J (2013) PDMS/single-walled carbon nanotube composite for proton radiation shielding in space applications. *Mater Lett* 108:79–83
- [15] Nambiar S, Yeow JT (2012) Polymer-composite materials for radiation protection. *ACS Appl Mater Interfaces* 4(11):5717–5726
- [16] Najafi E, Shin K (2005) Radiation resistant polymer–carbon nanotube nanocomposite thin films. *Colloids Surf A Physicochem Eng Asp* 257:333–337
- [17] Bhowmik S, Benedictus R, Poullis H, Bonin H, Bui VT (2009) High-performance nanoadhesive bonding of space-durable polymer and its performance under space environments. *J Spacecr Rockets* 46(1):218–224
- [18] Hashimoto N, Oie S, Homma H, Ohnuki S (2014) In situ observations of microstructure evolution in electron-irradiated multi-wall carbon nanotubes. *Mater Trans* 55(3):458–460
- [19] Chen S et al (2014) Polymer nanocomposite for space applications. In: 2014 IEEE 14th international conference on nanotechnology (IEEE-NANO), pp 685–688. IEEE
- [20] Li L, Su J, Zhu X (2016) Non-uniform shrinkage of multiple-walled carbon nanotubes under in situ electron beam irradiation. *Appl Phys A* 122(10):912
- [21] Li Z et al (2016) PMMA/MWCNT nanocomposite for proton radiation shielding applications. *Nanotechnology* 27(23):234001
- [22] Yang J, Li X, Liu C, Rui E, Wang L (2015) Effects of electron irradiation on LDPE/MWCNT composites. *Nucl Instrum Methods Phys Res Sect B Beam Interact Mater Atoms* 365:55–60
- [23] McCaffrey J, Tessier F, Shen H (2012) Radiation shielding materials and radiation scatter effects for interventional radiology (IR) physicians. *Med Phys* 39(7):4537–4546
- [24] Cho J, Kim M, Rhim J (2015) Comparison of radiation shielding ratios of nano-sized bismuth trioxide and molybdenum. *Radiat Effects Defects Solids* 170(7–8):651–658
- [25] Ambika MR, Nagaiah N, Suman S (2017) Role of bismuth oxide as a reinforcer on gamma shielding ability of unsaturated polyester based polymer composites. *J Appl Polym Sci* 134(13):44657
- [26] Cengel KA, Diffenderfer ES, Avery S, Kennedy AR, McDonough J (2010) Using electron beam radiation to simulate the dose distribution for whole body solar particle event proton exposure. *Radiat Environ Biophys* 49(4):715–721
- [27] Nambiar S, Osei EK, Yeow JTW (2013) Polymer nanocomposite-based shielding against diagnostic X-rays. *J Appl Polym Sci* 127(6):4939–4946
- [28] Yao Y et al (2016) Investigation of gamma ray shielding efficiency and mechanical performances of concrete shields containing bismuth oxide as an environmentally friendly additive. *Radiat Phys Chem* 127:188–193
- [29] Maghrabi HA, Vijayan A, Deb P, Wang L (2016) Bismuth oxide-coated fabrics for X-ray shielding. *Text Res J* 86(6):649–658
- [30] Fu SY, Feng XQ, Lauke B, Mai YW (2008) Effects of particle size, particle/matrix interface adhesion and particle loading on mechanical properties of particulate–polymer composites. *Compos Part B Eng* 39(6):933–961
- [31] Fan Z, Gong F, Nguyen ST, Duong HM (2015) Advanced multifunctional graphene aerogel–poly (methyl methacrylate) composites: experiments and modeling. *Carbon* 81:396–404
- [32] Shen JN, Yu CC, Ruan HM, Gao CJ, Van der Bruggen B (2013) Preparation and characterization of thin-film nanocomposite membranes embedded with poly (methyl methacrylate) hydrophobic modified multiwalled carbon nanotubes by interfacial polymerization. *J Membr Sci* 442:18–26
- [33] Weng B, Xu F, Salinas A, Lozano K (2014) Mass production of carbon nanotube reinforced poly (methyl methacrylate) nonwoven nanofiber mats. *Carbon* 75:217–226
- [34] Wang SX, Jin CC, Qian WJ (2014) Bi₂O₃ with activated carbon composite as a supercapacitor electrode. *J Alloys Compd* 615:12–17

- [35] Trivedi MK et al (2015) Evaluation of atomic, physical, and thermal properties of bismuth oxide powder: an impact of biofield energy treatment. *Am J Nano Res Appl* 3(6):94–98
- [36] Thirsk R, Kuipers A, Mukai C, Williams D (2009) The space-flight environment: the International Space Station and beyond. *Can Med Assoc J* 180(12):1216–1220
- [37] Martel-Estrada S, Santos-Rodríguez E, Olivás-Armendáriz I, Cruz-Zaragoza E, Martínez-Pérez C (2014) The effect of radiation on the thermal properties of chitosan/mimosa tenuiflora and chitosan/mimosa tenuiflora/multiwalled carbon nanotubes (MWCNT) composites for bone tissue engineering. In: *AIP conference proceedings*, vol 1607, no. 1, pp 55–64. AIP
- [38] Varela-Rizo H, Bittolo-Bon S, Rodríguez-Pastor I, Valentini L, Martín-Gullón I (2012) Processing and functionalization effect in CNF/PMMA nanocomposites. *Compos Part A Appl Sci Manuf* 43(4):711–721
- [39] Velasco-Santos C, Martínez-Hernández AL, Fisher FT, Ruoff R, Castano VM (2003) Improvement of thermal and mechanical properties of carbon nanotube composites through chemical functionalization. *Chem Mater* 15(23):4470–4475
- [40] Petersen EJ et al (2014) Methods to assess the impact of UV irradiation on the surface chemistry and structure of multi-wall carbon nanotube epoxy nanocomposites. *Carbon* 69:194–205
- [41] Singh D et al (2010) Radiation induced modification of dielectric and structural properties of Cu/PMMA polymer composites. *J Non Cryst Solids* 356(18–19):856–863
- [42] Suarez JC, Mano EB, Da Costa Monteiro EE, Tavares MI (2002) Influence of γ -irradiation on poly (methyl methacrylate). *J Appl Polym Sci* 85(4):886–895
- [43] Kratky P et al Impact of irradiation dose on mechanical properties of PMMA. *Latest Trends Syst* 1:290
- [44] Arshak K, Korostynska O (2006) *Advanced materials and techniques for radiation dosimetry*. Artech House, Boston
- [45] Hu N, Karube Y, Yan C, Masuda Z, Fukunaga H (2008) Tunneling effect in a polymer/carbon nanotube nanocomposite strain sensor. *Acta Mater* 56(13):2929–2936